RSC Advances

PAPER

View Article Online
View Journal | View Issue

Cite this: *RSC Adv.*, 2020, **10**, 37028

Enhanced visible light photocatalytic degradation of dyes in aqueous solution activated by HKUST-1: performance and mechanism†

Jianyu Zhang,[a] Chunli Su,*[a] Xianjun Xie,[a] Peng Liu[a] and Md. Enamul Huq[b]

HKUST-1 is a copper-based metal–organic framework (MOF) and potential photocatalyst, but minimal research has addressed the performance and mechanism of HKUST-1 in the visible light photocatalytic degradation of dyes. In the present work, HKUST-1 was applied as a photocatalyst to activate peroxomonosulfate (PMS) under visible light (Vis) for dye removal in aqueous solution. The results showed that the removal efficiency of two cationic dyes [rhodamine B (RhB) and methylene blue (MB)] was greater than 95% within 120 min. Free radicals such as $SO_4^{-\bullet}$, ·OH were present in the degradation process, with $SO_4^{-\bullet}$ playing a dominant role. Zeta potential, X-ray photoelectron spectroscopy, and photoluminescence spectroscopy data were used to investigate the degradation mechanism. In the degradation process, surface charge attraction between HKUST-1 and cationic dyes promotes removal efficiency, with the degradation efficiency of cationic dyes (MB and RhB) more than 50% higher than for anionic dyes [acid orange 7 (AO_7) and methyl red (MR)]. On the other hand, HKUST-1 has been proved to activate PMS by conducting photoelectrons, which accelerated the degradation of dyes. Compared with the reaction conditions of PMS/Vis, when the HKUST-1 was present (HKUST-1/PMS/Vis), the degradation rates of MB and RhB increased by 62.7 and 63.2%, respectively.

Received 16th June 2020
Accepted 4th September 2020

DOI: 10.1039/d0ra05275b

rsc.li/rsc-advances

1. Introduction

Traditional industries such as dyestuffs, textiles, and paper inevitably release a large amount of dyes into wastewater. The total amount of dyestuff and pigments produced worldwide is over 700 000 metric tons per year,[1] but nearly 10–15% of the dyes enter wastewater streams during manufacturing and processing.[2] The high chroma, poor biodegradability, and high toxicity of dye wastewater pose serious threats to human and environmental health.[3,4]

Common methods for treating dye wastewater include adsorption, filtration, and membrane treatment.[5] However, the removal efficiency achieved are still insufficient and these methods often have associated with safety risks.[6,7] Photolysis is an effective advanced oxidation method for treating dye wastewater, employing photocatalysts to convert light energy into chemical energy that then degrades dyes into small molecules.[8] Traditional photocatalysts including TiO_2, CdS, and Ag, among others have challenges in terms of efficiency and economics that remain to be overcome. Recently, copper-based photocatalysts have received much attention in the field of photolysis due to their excellent performance and relatively low cost.[9] Tian *et al.* synthesized Cu_2O/Cu composites that were applied to the photolysis of methyl blue (MB) in water, with a degradation rate of 87.74% achieved within 80 min.[10] Mosleh, Rahimi *et al.* synthesized CuO/Cu_2O/Cu composites and photodegraded MB in aqueous solution with the assistance of ultrasound, with the degradation efficiency reaching 91.91% within 90 min.[11]

Metal–organic frameworks (MOFs) are a type of semiconductor formed by the complexation of metals or metal clusters with organic ligands.[12] Recently, a copper-based MOF known as HKUST-1 has attracted extensive attention and is one of the few commercially available MOFs.[13]† HKUST-1 is formed by the coordination of Cu^{2+} and trimesic acid (H_3BTC), and has large specific surface area and high porosity. The research to date on HKUST-1 mainly focuses on hydrogen storage and CO_2 adsorption, and limited research has investigated HKUST-1 as a potential copper-based photocatalyst for the photodegradation of dyes.[14–16] Therefore, this study examined the performance and mechanism of HKUST-1 in the visible light (Vis) degradation of dyes. Permonosulfate (PMS) was selected as the electron acceptor and used to establish an HKUST-1/PMS/Vis system to enhance the photolysis. Four dyes [rhodamine B (RhB), methylene blue (MB), methyl red (MR), and acid orange 7 (AO_7)] were selected as the degradation targets. Differences in degradation performance for the four dyes by HKUST-1/PMS/Vis were determined and the removal mechanism was investigated. Influential factors such as dosage and initial pH were also considered.

[a]*School of Environmental Studies, China University of Geosciences, Wuhan, 430074, China. E-mail: chl.su@cug.edu.cn; Fax: +86-27-87481030; Tel: +86-27-67883170*

[b]*State Key Laboratory for Information Engineering in Surveying Mapping and Remote Sensing, Wuhan University, Wuhan 430079, China*

† Electronic supplementary information (ESI) available. See DOI: 10.1039/d0ra05275b

2. Materials and methods

2.1 Preparation of HKUST-1

HKUST-1 was synthesized using the solvothermal method.[17] First, 1.95 g of $Cu(NO_3)_2 \cdot 2.5H_2O$ (>99%) and 1.0 g of trimesic acid (H_3BTC) were dissolved in 51 mL of mixed solvent (water : ethanol : *N*,*N*-dimethylformamide in a 1 : 1 : 1 volume ratio). After stirring for 10 min, the mixture was poured into a Teflon-lined autoclave vessel and heated in an oven at 120 °C for 20 h. The mixture then was cooled to room temperature and washed with ethanol and deionized water five times to obtain the blue solid, which was dried at 100 °C for 12 h before use.

2.2 Characterization method

HKUST-1 was examined using X-ray diffraction (XRD) (D8-FOCUS, Bruker AXS, Germany) and Fourier-transform infrared spectroscopy (Nicolet 6700, Thermo Fisher, USA). The morphology of as-synthesized HKUST-1 was characterized by scanning electron microscopy (SEM) (SU8010, Hitachi, Japan). Elemental valence analysis and electronic cloud state were determined with X-ray photoelectron spectroscopy (XPS) (EscaLab 250Xi, Thermo, USA). Diffuse reflectance spectra (DRS) data were obtained using a UV-Vis spectrometer (UV-2550PC, Shimadzu, Japan). Zeta potentials were determined by a potentiometric analyzer (Nano ZS90, Malvern, UK). BET data were recorded with a pore size and fully automatic analyzer (ASAP2460, Micromeritics, USA). Photoluminescence (PL) spectroscopy was conducted using a fluoro spectrophotometer (F-4600, Hitachi, Japan). The valence band potential of the material was determined by ultraviolet photoelectron spectroscopy (UPS) (EscaLab 250Xi, Thermo, USA).

2.3 Photocatalytic degradation of dyes (RhB, MB, AO_7, MR)

The performance of the HKUST-1/PMS/Vis system was evaluated in terms of the degradation of both cationic dyes (RhB and MB) and anionic dyes (AO_7 and MR). For batch experiments, HKUST-1 and PMS were put into 100 mL of aqueous dye solution (10 mg L^{-1}), then the light source turned on and stirring commenced to start the reaction. The visible light source (400–800 nm) was a tungsten halogen lamp (QVF135/500 W). The stirring speed and temperature were constant at 500 rpm and 24 °C, respectively. During the reaction, 6 mL of the mixture were taken out at regular intervals (15, 30, 60, 90, 120, 150, 180 min) and filtered (0.22 μm), with the dye concentrations measured with an ultraviolet spectrophotometer (DR2800, HACH). The initial pH of the mixture was adjusted using NaOH (0.1 mol L^{-1}) or HNO_3 (0.1 mol L^{-1}), and measured by a pH electrode (9157BNMD, Thermo Scientific, USA).

3. Results and discussion

3.1 Characterization of the HKUST-1

XRD data were used to characterize the crystal structure of HKUST-1. Fig. 1a shows the spectrum had good peak shapes, with several peaks (*e.g.*, 200, 220, 222, 400, 333) consistent with previously recorded spectra.[18] Fig. 1b is the FT-IR spectra of HKUST-1, which features a broad peak around 3000–3500 cm^{-1} corresponding to the stretching vibration mode of the hydroxyl group in the water molecule. The band at around 729 cm^{-1} represents the Cu–O bond and confirms the coordination of Cu^{2+} and –COOH.[19] Organic ligands can act as electron-conducting media and form an electron transport chain from organic ligands to transition metals, so the coordination of Cu–O will favor the catalytic performance of HKUST-1.[20] The band at 1371 cm^{-1} corresponds to the C=C stretching vibration of benzene.[21] The peak at 1643 cm^{-1} is attributed to C=O stretching in the carboxyl group. Fig. 1c presents the SEM and the corresponding energy dispersive X-ray spectroscopic (EDS) images of HKUST-1. HKUST-1 displayed a regular octahedral shape, consistent with previous studies of its morphology.[22] In addition, the EDS elemental analysis revealed that the main elements present were Cu, O, and C, also confirming the successful synthesis of HKUST-1 (Fig. 1d).

The zeta potential test was applied to characterize the surface charge properties of HKUST-1 as these will have an important effect on the photocatalytic degradation process by way of surface charge action. Fig. 2a shows the potential of HKUST-1 is negative from pH 2 to 11, indicating the surface of HKUST-1 is negatively charged and therefore more prone to attract cations on micro surfaces; this may be beneficial for the removal of cationic dyes. BET characterization was carried out to determine the specific surface area, pore size, and pore volume of HKUST-1 (Fig. 2b). The large specific surface area (1215.91 $m^2 g^{-1}$) will provide more active reactive sites and favor enhanced photodegradation efficiency. However, the average pore size and pore volume are small (2.05 nm, 0.07 $cm^3 g^{-1}$), and the N_2 adsorption–desorption curve shows a I/II mixed type isotherm; this indicates HKUST-1 has a mesoporous structure that may weaken the adsorption of dyes. UV-Vis diffuse reflectance spectroscopy (DRS) was used to characterize the optical properties of HKUST-1. Fig. 2c shows HKUST-1 absorbed light in both the ultraviolet and visible regions. The band gap energies of HKUST-1 were calculated using the following equation:

$$(\alpha h\nu)^2 = A(h\nu - E_g) \quad (1)$$

where α, h, ν, and E_g are the absorption coefficient, Planck's constant, light frequency, and band gap energy, respectively. The value of the band gap energy is the *x*-intercept of a plot of $(\alpha h\nu)^2$ *versus* photon energy ($h\nu$), which for HKUST-1 was determined to be 3.31 eV. UV photoelectron spectroscopy (UPS) was used to characterize the valence band of HKUST-1 (Fig. 2d). The valence and conduction band (CB) were determined to be 3.1 V and −0.21 V *versus* the normal hydrogen electrode (NHE), respectively.

Where α, h, ν, and E_g are absorption coefficient, Planck's constant, light frequency, and band gap energy, respectively. The value of the band gap energy is the intersection of the plots of $(\alpha h\nu)^2$ *versus* photon energy ($h\nu$) and the *X* axis. The band gap energies of the HKUST-1 was calculated as 3.31 eV. UV photoelectron spectroscopy (UPS) test was applied to characterize the valence band of HKUST-1 (Fig. 2d), and the valence band energy

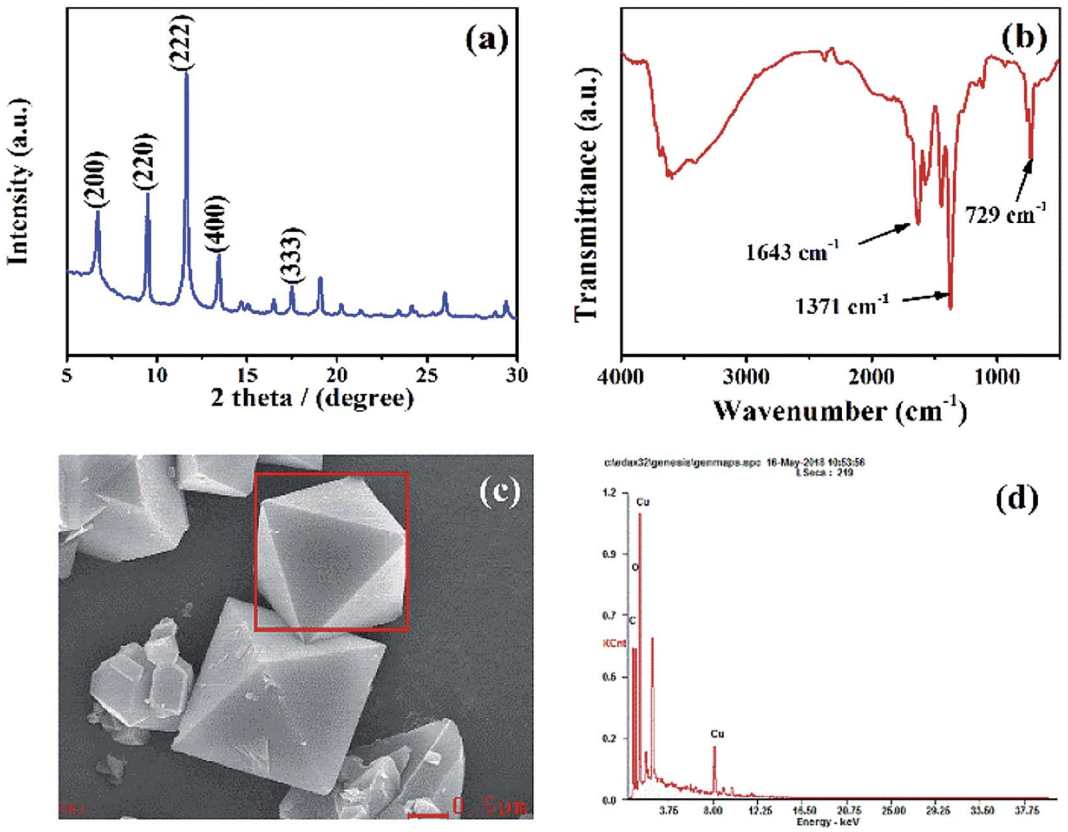

Fig. 1 XRD pattern (a), FT-IR spectra (b), SEM (c) and EDS images (d) of HKUST-1.

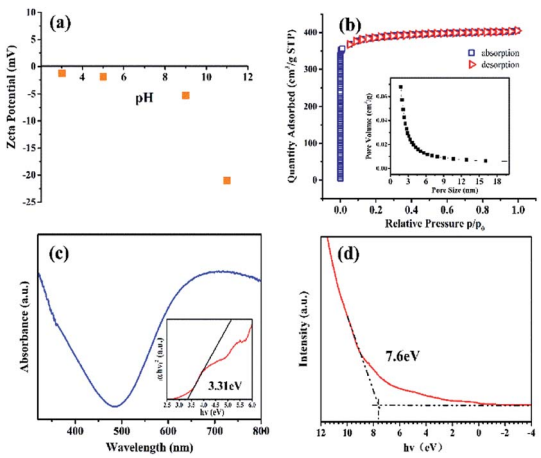

Fig. 2 Zeta potential (a), N_2 adsorption–desorption curve (b), DRS (c) and UPS data (d) of HKUST-1.

was determined to be 2.3 V *versus* NHE, so the conduction band of HKUST-1 is −1.01 V *versus* NHE.

3.2 Photocatalyst degradation of dyes (RhB, MB, AO_7 and MR)

Cationic dyes RhB and MB and anionic dyes AO_7 and MR were selected as the degradation targets to evaluate the performance of HKUST-1/PMS/Vis. Fig. 3 shows the removal of dyes under different conditions, including (1) HKUST-1/dark or Vis; (2) PMS/dark or Vis; and (3) HKUST-1/PMS/dark or Vis.

When the reaction condition was HKUST-1/dark or Vis, removals of AO_7, MR, and RhB were all less than 10%. Because the forbidden band of HKUST-1 (3.31 eV) exceed the theoretical minimum energy that can be excited by visible light (3.1 eV), the removal rate of these dyes was low. The removal of MB reached

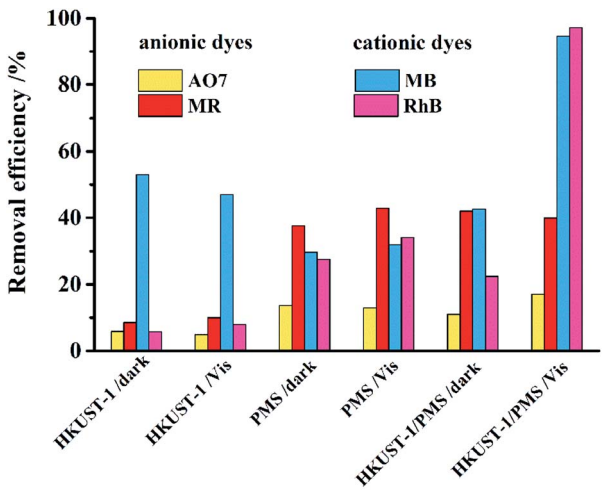

Fig. 3 Photocatalytic degradation of cationic dyes RhB, MB and two anionic dyes AO_7, MR.

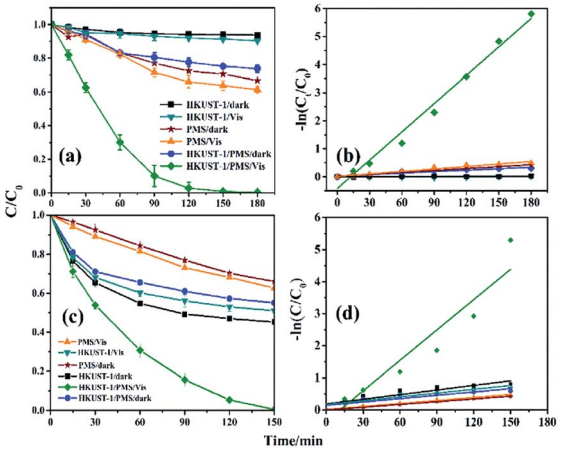

Fig. 4 Degradation kinetics under six degradation conditions (a) and pseudo-first-order kinetic curve (b) of RhB; degradation kinetics under six degradation conditions (c) and pseudo-first-order kinetic curve (d) of MB.

50%, which was attributed to adsorption by HKUST-1. When the reaction condition was PMS/dark or Vis, none of the removal rates exceeded 50%, indicating PMS has a low efficiency in terms of dye degradation. Finally, when the reaction condition was HKUST-1/PMS/Vis, the degradation of MB and RhB reached 95% due to the synergistic effect of HKUST-1, PMS, and visible light. However, the removal efficiency of AO_7 and MR was lower than 40%, which may be due to the surface charge repulsion of anionic dyes by HKUST-1. The degradation of MB and RhB for HKUST-1/PMS/Vis conditions was 51.9% and 74.8% higher than for HKUST-1/PMS/dark conditions, confirming the importance of visible light in the system. The adsorption of HKUST-1 on MB reached 53%, while the adsorption on RhB was only 5.8%; this may be attributed to the small pore size (2.05 nm) and pore volume (0.07 $cm^3\ g^{-1}$) of HKUST-1. However, this did not affect the degradation efficiency of the two cationic dyes by the HKUST-1/PMS/Vis system.

3.3 Degradation of dyes in different catalytic conditions

Kinetic curves can provide more detailed information about the photodegradation process of the dyes. Considering that the treatment effect of RhB and MB was better, they were chosen for the degradation kinetics experiments. The adsorption equilibrium curves of RhB and MB are shown in Fig. S1 and S2.† HKUST-1 has little adsorption on RhB, while the adsorption rate for MB is higher (55%), although the rate is relative slow. The effects of dosage of agent and initial pH on the degradation of RhB were also explored. Fig. 4a illustrates the kinetic curve of RhB under different degradation conditions. The degradation of RhB can reach 70% and 90% within 60 and 90 min, respectively (HKUST-1/PMS/Vis), but the degradation efficiency decreased with decreasing RhB concentration. The degradation kinetic curve of RhB satisfies a pseudo first-order kinetic model (Fig. 4b). The kinetic curve was established according to eqn (2) and (3):

$$d_c/d_t = -kc \quad (2)$$

$$\ln(c_t/c_0) = -kt \quad (3)$$

where k, c_t, and c_0 represent the rate constant, concentration of RhB, and initial concentration of RhB, respectively. The correlation coefficient was 0.985 and the value of k was 0.0337 min^{-1} (HKUST-1/PMS/Vis). The degradation kinetic curve and pseudo first-order kinetic curve of methylene blue are shown in Fig. 4c and d, respectively. Dosage of agents is a fundamental factor for practical applications, so the effect of dosage on RhB degradation was investigated by adjusting the mass ratio of HKUST-1 to PMS (Fig. S3†). Enhancement of the mass ratio of HKUST-1 and PMS affects the degradation efficiency of RhB: the degradation rate of RhB significantly improved when the ratio increased from 1 : 1 to 2 : 1; further improvement of RhB degradation was not obvious when the ratio was increased to 4 : 1; and the degradation of RhB was lower at a 5 : 1 ratio than a 4 : 1 ratio. This phenomenon can be attributed to the effect of excess HKUST-1 creating turbid conditions and hindering both the penetration of light and production of free radicals. Moreover, the reduction in the utilization of light energy led to a decline in the capacity of HKUST-1/PMS/Vis to degrade RhB. Therefore, in consideration of economic aspects when comparing treatment effects, a 2 : 1 ratio of HKUST-1 : PMS is the best choice for RhB degradation.

The effect of initial pH on the degradation of RhB is shown in Fig. S4.† The degradation rate of RhB was approximately 95% over a wide pH range (3–11) within 120 min, indicating the change of initial pH had little effect on the degradation of RhB. The degradation of RhB was markedly less at an initial pH of 1, as the structure of HKUST-1 collapsed. The catalytic process stopped when the HKUST-1 decomposed, indicating its role in the heterogeneously catalyzed process. It also positively reflects the importance of HKUST-1 for RhB degradation.

3.4 Degradation mechanism

During the photocatalytic degradation process, free radicals played a major role. Free radicals in the system were identified through scavenging action by quenchers (Fig. 5). Benzoquinone

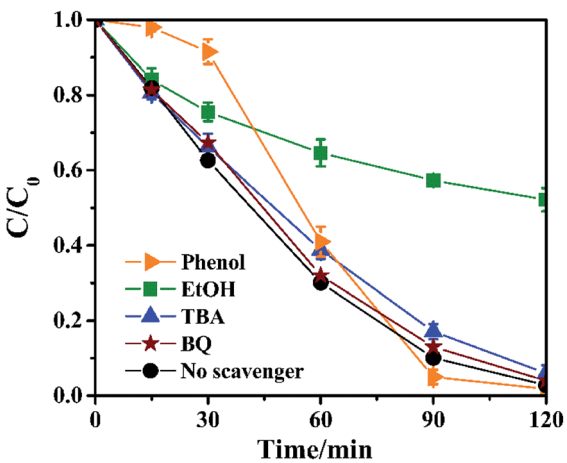

Fig. 5 The degradation of RhB in the presence of radical scavengers (experiment conditions: RhB = 10 ppm; HKUST-1 = 0.40 g L^{-1}; PMS = 0.20 g L^{-1}).

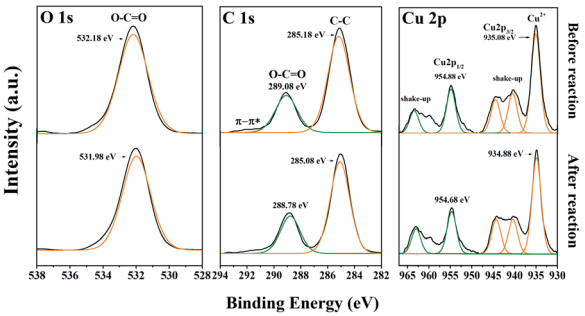

Fig. 6 The XPS of HKUST-1 in the range of O 1s, C 1s and Cu 2p for that before (pristine) and after reaction (degradation on RhB).

(BQ) is a common scavenger for quenching $\cdot O^{2-}$.[23] Fig. 5 shows the photodegradation of RhB was almost unaffected when BQ was present, indicating that the $\cdot O^{2-}$ had little effect in the system. Tertiary butanol (TBA) and ethanol (EtOH) are typical radical scavengers. EtOH is recognized as a capturer for $SO_4^{-\cdot}$ and ·OH, while TBA mainly quenches ·OH in solution and weakly scavenges $SO_4^{-\cdot}$.[24] Fig. 5 shows the degradation of RhB was significantly inhibited when EtOH was present, while TBA did not have a major inhibitory effect. This confirms $SO_4^{-\cdot}$ is the main oxidizing free radical and ·OH plays a minor role. In the HKUST-1/PMS/Vis system, $SO_4^{-\cdot}$ was only generated by the activation of PMS. The generation process of $SO_4^{-\cdot}$ from PMS is as follows:

$$HSO_5^- + e^- \rightarrow (SO_4^{-\cdot} + OH^-) \text{ or } (SO_4^{2-} + \cdot OH) \quad (4)$$

Phenol is a common scavenger of $SO_4^{-\cdot}$ and ·OH, and the hydrophobicity of phenol makes it more inclined to associated with the surface of the catalyst.[25] When phenol was present, the degradation rate of RhB was significantly reduced in the first 30 min due to the scavenging effect, and then gradually recovered over the next 30 min. This phenomenon may due to the volatilization of phenol and a reduction in the scavenging effect of $SO_4^{-\cdot}$ and ·OH on the surface of HKUST-1, resulting in the gradual recovery of the degradation efficiency of RhB. It also indirectly demonstrated the photodegradation of RhB by HKUST-1/PMS/Vis is a heterogeneous catalytic process.

Fig. 6 presents the XPS spectra of HKUST-1 (before and after reaction). The O 1s spectra has a peak at 532.18 eV, which is assigned to the carboxylate groups (O–C=O) in HKUST-1.[26] After photocatalytic degradation, the binding energy of the O–C=O shifts to 531.98 eV, which is 0.2 eV less than for HKUST-1 (before reaction). The Cu 2p spectrum features peaks at 954.88 and 935.08 eV, associated with Cu $2p_{1/2}$ and Cu $2p_{3/2}$.[27] After the reaction, the binding energy of these peaks shift to 954.68 and 934.88 eV, respectively, both of which are 0.2 eV less than for the HKUST-1 before the reaction. The C 1s signal from HKUST-1 is derived from the H_3BTC; the two peaks at 289.08 and 285.18 eV are attributed to C–C in the benzene ring and O–C=O in –COOH, respectively.[28] Probably because the "O" on –COOH has a strong electronegativity, so it has a strong ability to attract electrons. After the reaction, the binding energy of these two C 1s peaks shifted to 288.78 and 285.08 eV, respectively, which are respectively 0.3 and 0.1 eV less than for HKUST-1 before the reaction. In general, the binding energies of O 1s, C 1s, and Cu 2p all shifted to lower values after the reaction; these reductions may be due to the increasing electron cloud density of organic ligands and metal centers.[27] Although the binding energies all decreased, the extent of the decline differed. The maximum binding energy shift was for O–C=O (0.3 eV), followed by Cu–O (0.2 eV), indicating the coordination units of –COOH and Cu^{2+} captured more photoelectrons, while the benzene ring contributes less due to the smaller change in electron cloud density (0.1 eV). Analysis of the XPS results indicates HKUST-1 acts as an electron capture and transfer medium in the photocatalytic degradation process.

The C_B of HKUST-1 is −0.21 V *versus* NHE, which is more negative than the redox potential of PMS, and the electrons on the C_B of HKUST-1 can activate PMS in theory.[29] Therefore, PL spectroscopy was applied to verify whether free electrons on the C_B of HKUST-1 can activate PMS. Fig. 7 shows that the fluorescence intensity decreases when PMS is present, indicating PMS weakens the recombination of photo-generated electrons and has the ability to acquire electrons from the C_B of HKUST-1.

Taken together, the results of the free radical identification, XPS analysis, and PL spectroscopy investigation indicate the degradation mechanism should be as follows. With the stimulation of visible light, the dyes generate photoelectrons due to their own photosensitivity, and through charge attraction contact the HKUST-1 surface and transfer photoelectrons to the C_B of HKUST-1. PMS obtains photoelectrons from HKUST-1 and accelerates self-decomposition to generate $SO_4^{-\cdot}$ and ·OH, which then degrade MB and RhB. Due to repulsion between the anionic dyes (AO_7, MR) and surface charges of HKUST-1, photoelectron transfer to HKUST-1 is difficult and, in turn, PMS is not activated to trigger the degradation process (Fig. 8).

Recyclability is an important consideration when evaluating the practical application of materials. Fig. 9a shows that over 75% degradation of RhB is still achieved after four cycles. The 20% decline in degradation after five cycles can be attributed to

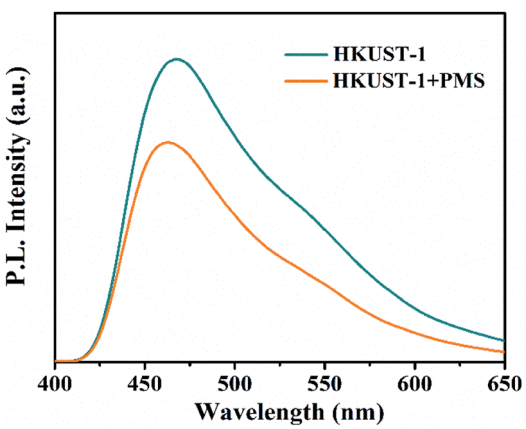

Fig. 7 Photoluminescence spectra (PL) of HKUST-1 and HKUST-1/PMS.

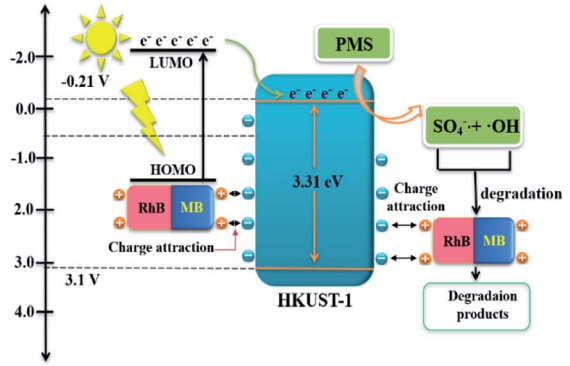

Fig. 8 Plausible mechanism of photocatalytic degradation of RhB and MB by HKUST-1/PMS/Vis.

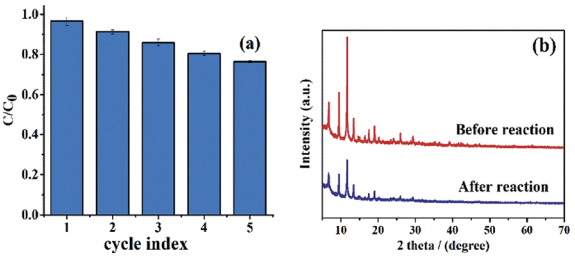

Fig. 9 Reusability of the HKUST-1 for the degradation of RhB (a); XRD patterns of HKUST-1 before and after the reaction (b).

the loss of material. Fig. 9b shows XRD patterns of HKUST-1 before and after the reaction. After the reaction, the characteristic peak intensity of HKUST-1 slightly decreased, but the characteristic peak remained unchanged and no hetero peak appeared, indicating HKUST-1 has stable chemical properties and the HKUST-1/PMS/Vis system has the capacity to work cyclically.

4. Conclusions

The experimental results showed that the HKUST-1/PMS/Vis system can effectively degrade the dyes, and HKSUT-1/PMS/Vis had good selectivity for the degradation of cationic dyes (RhB and MB) and poor degradation of anionic dyes (AO_7 and MR). The HKUST-1/PMS/Vis system effectively degraded RhB and MB but accomplished poor removal of AO_7 and MR, which is attributed to the repulsion between surface charges. DRS, XPS, and PL analyses suggested injecting photoelectrons from dyes into HKUST-1 and activating PMS is the main route of HKUST-1/PMS/Vis degradation of dyes. In addition, data of DRS, XPS and PL confirmed that dyes injected photoelectrons into HKSUT-1 and activated PMS was the main route of HKUST-1/PMS/Vis degradation dyes.

Conflicts of interest

There are no conflicts to declare.

Acknowledgements

This research was supported by the Major Science and Technology Program for Water Pollution Control and Treatment "Research and demonstration of key technologies for water ecological environment remediation and water safety guarantee in Baiyangdian Lake and Daqing River Basin (Xiong'an New Area)" (2018ZX07110) and "Research and Engineering Demonstration of Groundwater Pollution Control and Remediation Technology for Typical Sewage Reclamation Ponds in Tanghe Sewage Reservoir and Xiong'an New Area" (2018ZX07110005).

Notes and references

1 S. Natarajan, H. C. Bajaj and R. J. Tayade, *J. Environ. Sci.*, 2018, **65**, 201–222.
2 P. V. Nidheesh, M. Zhou and M. A. Oturan, *Chemosphere*, 2018, **197**, 210–227.
3 F. Ahmedchekkat, M. S. Medjram and M. Chiha, *Chem. Eng. J.*, 2011, **178**, 244–251.
4 M. Jamshidi, M. Ghaedi, K. Dashtian, A. M. Ghaedi, S. Hajati, A. Goudarzi and E. Alipanahpour, *Spectrochim. Acta, Part A*, 2016, **153**, 257–267.
5 S. Mosleh, M. R. Rahimi, M. Ghaedi and K. Dashtian, *Ultrason. Sonochem.*, 2016, **32**, 387–397.
6 N. Ghows and M. H. Entezari, *Ultrason. Sonochem.*, 2013, **20**(1), 386–394.
7 M. Shirzad-Siboni, M. Farrokhi, R. D. C. Soltani, A. Khataee and S. Tajassosi, *Ind. Eng. Chem. Res.*, 2014, **53**(3), 1079–1087.
8 S. Mosleh, M. R. Rahimi, M. Ghaedi, K. Dashtian and S. Hajati, *RSC Adv.*, 2016b, **6**, 63667–63680.
9 J. Du, Y. Yuan, J. Sun, F. Peng, X. Jiang, L. Qiu, A. Xie, Y. Shen and J. Zhu, *J. Hazard. Mater.*, 2011, **190**, 945–951.
10 X. Y. Tian, J. Wen, Z. J. Chen, X. Liu, H. X. Peng, C. Y. Ji, J. Li, Y. X. Peng and H. P. He, *Solid State Sci.*, 2019, **93**, 70–78.
11 S. Mosleh, M. R. Rahimi, M. Ghaedi, K. Dashtian and S. Hajati, *Ultrason. Sonochem.*, 2018, **40**, 601–610.
12 Q. Zhu and Q. Xu, *Chem. Soc. Rev.*, 2014, **43**, 5468–5512.
13 J. A. Anderson, M. P. Singh, N. R. Dhumal, H. J. Kim and J. Kiefer, *J. Phys. Chem. C*, 2016, **120**(31), 17153–17862.
14 N. Torres, J. Galicia, Y. Plasencia, A. Cano, F. Echevarria, L. F. Desdin-Garcia and E. Reguera, *Colloids Surf., A*, 2018, **549**, 138–146.
15 C. L. Wang, Y. C. Su, X. L. Zhao, S. S. Tong and X. J. Han, *Chem.–Eur. J.*, 2018, **24**(5), 1080–1087.
16 H. M. Wen, B. Li, L. B. Li, R. B. Lin, W. Zhou, G. D. Qian and B. L. Chen, *Adv. Mater.*, 2018, **30**(16), 1704792.
17 Z. Hasan, J. Cho, J. Rinklebe, Y. S. Ok, D. W. Cho and H. Song, *J. Ind. Eng. Chem.*, 2017, **52**, 331–337.
18 K. Lin, A. K. Adhikari, C. N. Ku, C. L. Chiang and H. Kuo, *Int. J. Hydrogen Energy*, 2012, **37**, 13865–13871.
19 S. Lin, Z. Song, G. Che, A. Ren, P. Li, C. Liu and J. Zhang, *Microporous Mesoporous Mater.*, 2014, **193**, 27–34.
20 T. Zhang and W. Lin, *Chem. Soc. Rev.*, 2014, **43**, 5982–5993.
21 X. Yan, S. Komarneni, Z. Zhan and Z. Yan, *Microporous Mesoporous Mater.*, 2014, **183**, 69–73.

22 S. Mosleh, M. R. Rahimi, M. Ghaedi, K. Dashtian, S. Hajati and S. Wang, *Chem. Eng. Process.*, 2017, **114**, 24–38.
23 M. Mousavi, A. Habibi-Yangjeh, D. Seifzadeh, K. Nakata and S. Vadivel, *Adv. Powder Technol.*, 2019, **30**, 524–537.
24 T. Zeng, X. Zhang, S. Wang, H. Niu and Y. Cai, *Environ. Sci. Technol.*, 2015, **49**, 2350–2357.
25 J. Zhang, X. Shao, C. Shi and S. Yang, *Chem. Eng. J.*, 2013, **232**, 259–265.
26 K. Ahlenhoff, S. Koch, D. Emmrich, R. Dalpke, A. Golzhauser and P. Swiderek, *Phys. Chem.*, 2019, **21**, 2351–2364.
27 C. Chen, B. Li, L. Zhou, Z. Xia, N. Feng, J. Ding, L. Wang, H. Wan and G. Guan, *ACS Appl. Mater. Interfaces*, 2017, **9**, 23060–23071.
28 S. Y. Kim, A. R. Kim, J. W. Yoon, H. J. Kim and Y. S. Bae, *Chem. Eng. J.*, 2018, **335**, 94–100.
29 G. Zhou, H. Sun, S. Wang, H. M. Ang and M. O. Tade, *Sep. Purif. Technol.*, 2011, **80**, 626–634.